Enhanced Dynamic Response of DC-AC Converters in Shipboard Microgrids Using Non-linear PI Controller

Author(s): Naghash, Reza; Hassan, Mustafa Alrayah; Kauhaniemi, Kimmo; Laaksonen, Hannu

Title: Enhanced Dynamic Response of DC-AC Converters in Shipboard Microgrids Using Non-linear PI Controller

Year: 2025

Version: Accepted manuscript

Please cite the original version:

Naghash, R., Hassan, M. A., Kauhaniemi, K., & Laaksonen, H. (2025). Enhanced Dynamic Response of DC-AC Converters in Shipboard Microgrids Using Non-linear PI Controller. *IECON 2025 – 51st Annual Conference of the IEEE Industrial Electronics Society,* 1-6. IEEE. https://doi.org/10.1109/IECON58223.2025.11221792

Enhanced Dynamic Response of DC-AC Converters in Shipboard Microgrids Using Non-linear PI Controller

Reza Naghash
School of Technology and Innovations
University of Vaasa
Vaasa, Finland
reza.naghash@uwasa.fi

Mustafa Alrayah Hassan
School of Technology and Innovations
University of Vaasa
Vaasa, Finland
mustafa.alrayah.hassan.ibraheem@uwasa.fi

Kimmo Kauhaniemi
School of Technology and Innovations
University of Vaasa
Vaasa, Finland
kimmo.kauhaniemi@uwasa.fi

Hannu Laaksonen
School of Technology and Innovations
University of Vaasa
Vaasa, Finland
hannu.laaksonen@uwasa.fi

***Abstract*—This work presents a non-linear digital PI controller for DC-AC converters in shipboard microgrids (SMG) with hybrid energy storage systems (HESS), including battery and supercapacitor. The HESS power converters in SMG need fast and well-tuned dynamic response to ensure reliable operation in their distinctive load characteristics such as large variations in line voltage, load changes, and high degree of non-linearity. Conventional PI controllers prove their performance in most cases, however, due to their linear behaviour, they may fail to maintain all the control system parameters at desired ranges over the large and fast transients. To address this issue, a case study based on real mission profile of a hybrid ship is considered, and a non-linear PI controller with variable gains for different error values based on non-linear functions is introduced. Stability analysis based on frequency-domain and bode diagrams provides the improvement in dynamic response, and it is verified by simulation and controller hardware-in-the-loop (CHIL) tests.**

***Index Terms*—DC-AC Converters, Non-linear PI Controller, Adaptive Control, Fast Dynamic Response, CHIL Test, Shipboard Microgrids, Hybrid Energy Storage Systems**

I. Introduction

Distinctive characteristics of shipboard microgrids (SMG) in all-electric ships (AES) cause their architecture to be different from terrestrial microgrids. One of the main characteristics of SMG is their load profile, and consequently, requirement for more advanced combinations of energy sources. In this regard, Hybrid Energy Storage Systems (HESS) are utilized to tackle complex load behaviors such as high share of non-linear loads, pulsed loads, intermittent loads, and regenerative loads [1].

To respond to the mentioned load profile, there is a need for a combination of energy storage systems with both high power density and high energy density to provide a reliable generation. Today's HESS mainly consists of battery energy storage systems (BESS) and supercapacitors, to be able to provide power for both short-term transients and long-term energy requirements. Providing power for short-term transient loads enables the need for more fast dynamic response energy storage interface converters [2]. The required response time for BESS is from few to 40ms, and 10-20ms for supercapacitors [1].

To comply with the response time of supercapacitors, the interface converters including DC-DC and DC-AC interface converters need to have fast and well-tuned dynamic response as well. Proper filter design alongside the conventional control methods can achieve this goal in most cases. Among conventional control methods, the linear proportional-integral (PI) control system is the most famous one, due to their simple implementation and zero steady-state error [3]. However, it may fail to maintain all the control parameters at the desired ranges for the fast dynamic response in all cases. To be more specific, due to the linearization, PI controller may fail to operate properly, especially in transients. This may lead to large overshoots and undershoots that are not seen in the linear model, or system instability [4].

Linear PI controller can be adjusted in the frequency-domain to minimize the error of measured variable and reference value. But due to the limitations of the linear controllers, such as low bandwidth and limited dynamic response especially for transient behaviour in large variations, non-linear controllers can be used. Hysteresis and geometric control methods are proposed to improve the transient response [6]. In addition to these well-known control systems, predictive control is also a suitable strategy to control power electronics converters. By using a discrete-time model and adjusting a cost function, Model Predictive Control (MPC) can be used

This research has received funding from the European Union's Horizon research and innovation programme under grant agreement no. 101095902 (AENEAS project).

to improve the dynamic response of power converters. MPC includes the nonlinearities of the system and the switch states of the converter are in their original form. Other desired constraints can be introduced to the cost function, which can guarantee the performance of the converter in all conditions. The main drawbacks of these non-linear methods are complexity, high computational demand, and model dependency [7], [8].

In this regard, to keep the advantage of linear PI controller while improving its poor transient response, non-linear PI controllers are introduced. While conventional PI feedback uses a linear combination of present and cumulative error terms, a non-linear combination employs non-linear functions, potentially offering better effectiveness [9]. This paper shows that with linear feedback terms, the error approaches zero in infinite time, whereas non-linear feedback terms in exponential forms enable the error to reach zero faster, in finite time. A non-linear digital proportional-integral-derivative (PID) controller for DC-DC converters is proposed in [10] to enhance the dynamic response of dual-phase synchronous buck converter for large error values. Instead of constant PID gains for all conditions, variable gains are designed for different error values, which dynamic response improved significantly. A self-tuning rule for PI gains design considering energy balance is provided in [11] for DC-AC converters. This method requires an additional energy balance algorithm. An adaptive PI controller with online tuning of PI gains based on fuzzy logic is proposed in [12] for three-phase voltage source inverters. This work needs additional efforts for calculating membership functions. A significant improvement in power quality and dynamic response for grid-connected inverters is provided in [13] utilizing an adaptive control. The improvement is shown during fast transients and sudden loads. The variable gains for the controller are optimized based on energy signal optimization, which makes it more complex. Besides research papers, non-linear PID controllers are of interest to industry. Texas Instruments provides a specific library to implement this technique in C2000 Digital Signal Processors (DSP) [14]. An application of this method in a Vienna rectifier is proposed in [15].

The literature proved that non-linear PI controllers can improve dynamic response significantly, however, there is still lack of proper design methodology, in-depth stability analysis, and digital implementation especially for DC-AC converters. Therefore, this paper focuses on proposing design process, frequency domain analysis, and digital implementation in a controller hardware-in-the-loop (CHIL) test for linear PI and non-linear PI for DC-AC converters using shipboard microgrid as a practical use case. Section II introduces shipboard microgrid design including power and conventional control stage as well as issues observed in the simulation. Section III proposes non-linear control system and frequency-domain analysis. Digital implementation and CHIL results are provided in section IV. Section V concludes the paper.

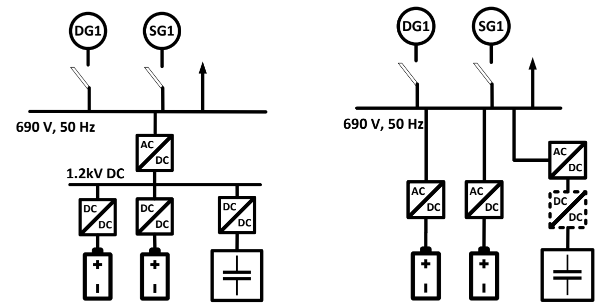

(a) Double stage DC-AC conversion with DC/AC buses

(b) Single stage DC-AC conversion with main AC bus

Fig. 1. Shipboard Microgrid with HESS.

II. Shipboard Microgrid Design

A. Power System

There are several topologies for SMG based on their main buses that can be DC, AC, or hybrid DC/AC [1]. Two simplified shipboard microgrids for this study is provided in Fig. 1. Diesel Generator (DG), Shaft Generator (SG), BESS, supercapacitor, and power converters are their main elements. It should be noted that the active front end (AFE) converters that are connected to the SG are not shown for simplicity. Figure 1(a) shows a SMG with main AC/DC buses that HESS are connected to the main AC bus through DC-DC and DC-AC converters. A SMG with main AC bus are provided in Fig. 1(b), in which the BESS are connected to the main AC bus with single-stage DC-AC converters. Due to the voltage decrease at the supercapacitor's terminals, A DC-DC converter is utilized usually, however, new design suggests eliminating this DC-DC converter to increase the efficiency of the system [16]. Hence, a single-stage conversion can also be used in this topology.

In the following, as the focus of the work is on controller design for DC-AC converters, the case study will be a portion of this SMG that includes supercapacitor, DC-DC and DC-AC converters, and AC generation source. The DC-AC converter is shown in Fig. 2. The AC bus voltage is 690 V - 50 Hz, and the DC voltage is set to 1.2 kV. The maximum power of the converter is set to 2 MW considering a real mission profile for the supercapacitors in a roll-on/roll-off (RORO) ship.

This converter utilizes an *LCL* filter in the output, to filter out the harmonics and ensure the controllability of the converter. The *LCL* filter is designed to attenuate the harmonics

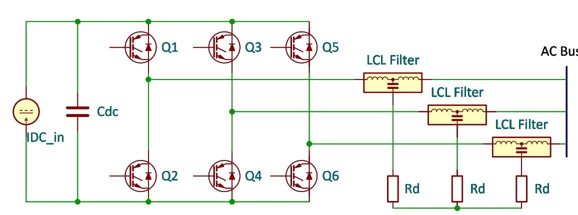

Fig. 2. DC-AC converter with *LCL* filter with passive damping.

and achieve desired current ripple reduction while limiting the AC voltage drop and maintaining high power factor [17]. The switching frequency is set to 4 kHz (2.5133e+04 rad/s), and minimum power factor assumed to be 0.995. To ensure stability, the resonance frequency is set to be around one-fourth of the switching frequency (6.2832e+03 rad/s), and the passive damping method is used in this case. This design is a reciprocal process, so the initial values are re-calculated in a few iterations to reach the proper values within the constraints. The final values of *LCL* filter are as follows:

$$L_1 = L_2 = 26.045\mu H, C_f = 2.1mF, R_d = 0.0174\Omega$$

Where, L_1, L_2, C_f, and R_d are inverter side inductor, AC side inductor, filter capacitance, and damping resistor, respectively. Considering filter parameters and switching frequency, the resonance frequency will be 6.0470e+03 rad/s. Besides, the required capacitance for DC bus is 50 mF.

B. Control System

The operational scenarios are an essential part for designing the control system for every converter in SMG. Therefore, the responsibility of converters vary across different ship operations including port-stay, manoeuvring, and navigation. Since the supercapacitors module as a fast response energy source is considered in this work, maoeveuring phase is studied, where the power demand is at peak value. In this mode, the DC-AC converter is responsible for injecting power to the AC bus alongside the DG and SG. Based on the power/energy management system, the DC-AC converter needs to operate in reverse direction to charge the supercapacitors module. This means that the converter needs to be able to control the discharged/charged current and DC bus voltage. To keep the generality of this work, a dual-loop control as shown in Fig. 3 is considered as the main control system. $G_i(s)$ is the inner loop transfer function $((G_{Filter(s)})(G_{delay}))$ and $G_{VI}(s)$ is the outer loop plant (output current to DC voltage transfer function). k_{FB1} and k_{FB2} are measurement, conditioning, and analog-to-digital converter (ADC) gains for inner and outer loops, respectively.

The voltage and current controller design are based on [18], [19]. First, the inner current loop is designed to set the Band-Width (BW) of the current loop to be half of the resonance frequency (1.2566e+04 rad/s). The single update mode is selected for sampling method, so the sampling time

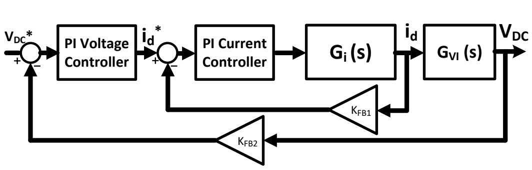

Fig. 3. Dual-loop control system for the DC-AC converter.

(T_s) is 250 µs. According to [19], the PI current controller coefficients are obtained by the following equations.

$$Kp_{currentloop} = \frac{0.33(L_1 + L_2)}{T_s} \tag{1}$$

$$Ti_{currentloop} = 10(T_s) \tag{2}$$

To design the voltage loop and ensure stability, the required BW for the voltage loop is set to be around one-tenth of the inner-loop, to get enough decoupling with inner-loop while having a fast enough response. By using equations in [18], the voltage loop transfer controller coefficients are derived based on the following equations.

$$Kp_{voltageloop} = \frac{0.02(C_{dc})}{T_s} \tag{3}$$

$$Ti_{voltageloop} = 17(T_s) \tag{4}$$

C. Analysis of Observed Problem

A simulation study with the design parameters is performed to validate the effectiveness of the controller design. In the first case, the input reference current is changed as shown in Fig. 4(a). The DC-link voltage and output current for phase A are stable and following the reference properly, in the specified response time. In the second case, a large variation is applied to the input current reference from 500 A to 2000 A, which frequently happens in the mission profile of the selected study. The corresponding results are shown in Fig. 4(b). It is observed that in large variation, the PI controller fail to work properly, and overshoot and undershoots are no longer in the specified range. The overshoot for small to large step changes varies from 4 % to 18 %. The settling time is also increased from 200 ms to 300 ms. In the next section, a non-linear PI controller is designed to address this issue.

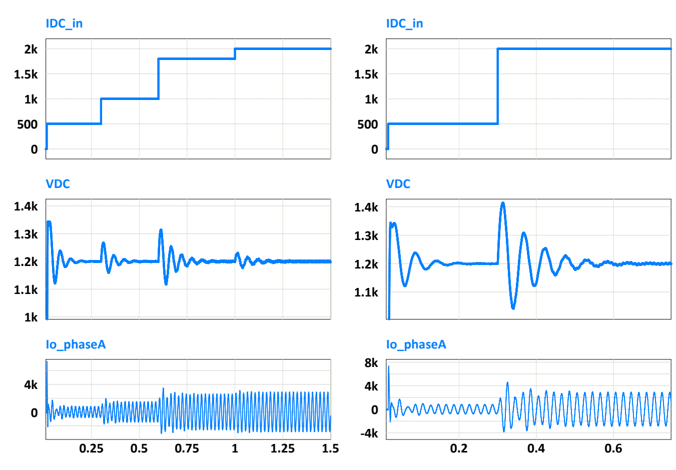

(a) Small step changes (b) Large step changes

Fig. 4. Simulation results for conventional PI controller.

III. Non-linear Control System

In this section, a non-linear digital PI controller is designed to replace the conventional controller presented in the previous section. The control system is depicted in Fig. 5. The controller

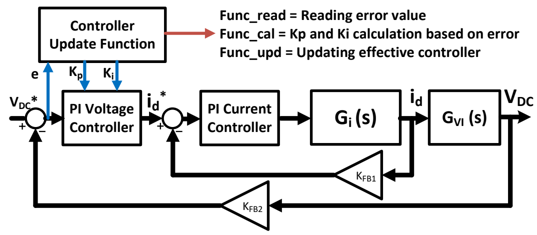

Fig. 5. Non-linear PI controller for dual-loop control system.

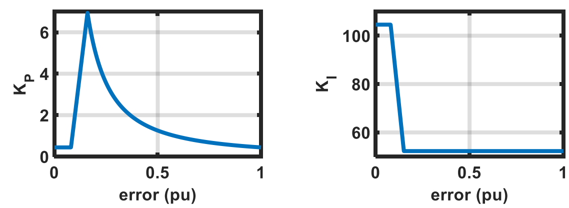

(a) Proportional gain vs error (pu) (b) Integral gain vs error (pu)

Fig. 6. PI coefficients for different error values.

update function consists of three main parts. The first part is a read function that receives the voltage error value. The second part is a calculation function that computes the PI gains based on the error value using predefined non-linear functions. Finally, the third part updates the controller coefficients to set the controller output to a desired value.

A. Controller Design

The general form of the PI controller in time-domain is provided in Eq. (5). Conventional PI uses constant gains for the feedback terms (K_p, K_i), whereas non-linear PI uses non-linear functions ($K_p(e)$, $K_i(e)$).

$$u(t) = K_p(e) \cdot e(t) + K_i(e) \cdot \int_0^t e(\tau)\, d\tau \tag{5}$$

With constant $K_p(e) = K_p$, the proportional term ($K_p \cdot e(t)$) is directly proportional to the error signal, which means it provides an immediate control response proportional to the magnitude of the error. Hence, increasing K_p makes the system to respond faster because the control action becomes larger for a given error. However, a too high proportional term pushes the system to higher overshoots and instability.

Considering the effects of proportional term in the PI controller, a non-linear function, $K_p(e)$, is designed to change the proportional gain based on the error values. The achieved function is proposed by Eq. (6), and plotted in Fig. 6(a) for $\alpha = 1.5$. Parameter α sets the degree of non-linearity of the function, in which $\alpha = 0$ means a constant gain for all errors. $a_{1,pu}$ and $b_{1,pu}$ are lower and upper per unit errors, that defines which part of the function should be selected for the proportional gain.

$$K_p(e) = \begin{cases} K_p, & 0 \le e < a_{1,\text{pu}} \\ m \cdot e + f_c, & a_{1,\text{pu}} \le e < b_{1,\text{pu}} \\ K_p \cdot e^{-\alpha}, & b_{1,\text{pu}} \le e \le 1 \end{cases} \tag{6}$$

Where

$$m = \frac{K_p \cdot b_{1,\text{pu}}^{-\alpha} - K_p}{b_{1,\text{pu}} - a_{1,\text{pu}}}$$
$$f_c = K_p - m \cdot a_{1,\text{pu}}$$

The integral term ($K_i \int_0^t e(\tau)\, d\tau$) accounts for the accumulation of past error values. So, it changes control output considering duration and magnitude of the error, and it increases over time to reduce the error to zero in steady-state. Too high integral gain leads to oscillations and instability in transient. Hence, a lower value for larger errors are considered for transient period to reduce oscillations. The function of integral gain can be obtained by Eq. 7. This function is plotted in Fig. 6(b) for $K_{i,\text{min}} = 0.5K_i$.

$$K_i(e) = \begin{cases} K_i, & 0 \le e < a_{1,\text{pu}} \\ m \cdot e + f_c, & a_{1,\text{pu}} \le e < b_{1,\text{pu}} \\ K_{i,\text{min}}, & b_{1,\text{pu}} \le e \le 1 \end{cases} \tag{7}$$

Where

$$m = \frac{K_{i,\text{min}} - K_i}{b_{1,\text{pu}} - a_{1,\text{pu}}}$$
$$f_c = K_i - m \cdot a_{1,\text{pu}}$$

For the proposed system, the calculated functions are derived based on a few iterations to ensure stable condition for all the operating point at all error values. The non-linear functions that are selected are depicted in Fig. 6. Stability analysis of these functions are provided in the next subsection.

B. Stability Analysis

To ensure proper tracking and stability of the system with variable PI gains, a frequency-domain analysis is provided based on the bode diagram of the loop function and closed loop transfer function of the outer loop. The bode diagrams are derived by varying α from 0 to 2, and per unit error from 0 to 1. The PI gains are calculated for each error value for 151 points, and the corresponding bode diagram is achieved, accordingly. To analyze the system, BW is obtained based on the closed-loop transfer function, and gain margin (GM) and phase margin (PM) are calculated by using loop-function. Results are provided in Fig. 7.

Figure 7(a) shows BW of closed-loop transfer function that indicates higher BW for higher α values in the defined range of errors ($a_{1,\text{pu}} \le e < b_{1,\text{pu}}$). This is because of increasing proportional term in those error values. This increase is more effective with higher values of α that are correlated to higher non-linearity in the system. According to this figure, it is expected that transient response time become faster. However, based on Figs. 7(b) and (c) that shows GM and PM of the loop function, the system will be close to instability for higher α. Considering frequency-domain analysis, proper value for α can be selected to have desired BW while having stable operation in all conditions.

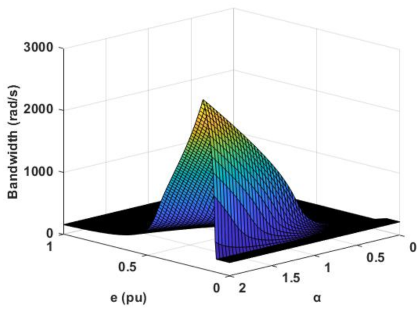

(a) Bandwidth

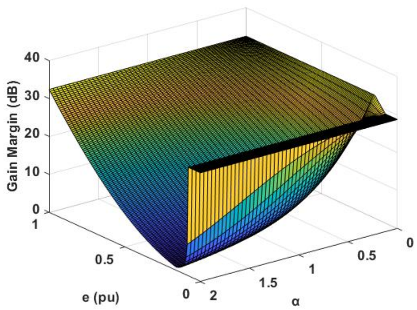

(b) Gain Margin

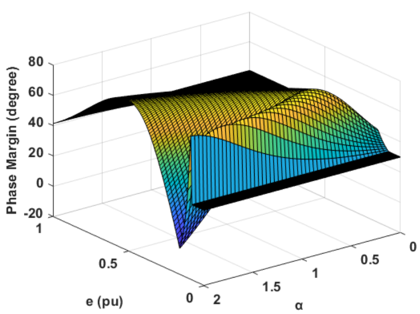

(c) Phase Margin

Fig. 7. Frequency-domain analysis of loop function and closed-loop response.

C. Simulation Results

To validate the effectiveness of the proposed non-linear controller, the controller code is rewritten considering the controller update function that is shown in Fig. 5. The controller update function is inserted after the phase-locked loop, and before applying the PI controller function to the error. First, new gains for both proportional and integral gains are calculated based on the predefined non-linear functions, and then the controller gains are updated and applied to the error at that instant.

Simulation results in the same case that is observed in Fig. 4(b) is provided in Fig. 8 for non-linear PI controller. A significant improvement in dynamic response can be observed. As shown in Fig. 8(a), the reference current is increased from 500 A to 2000 A that indicates the large variation in the system. The maximum overshoot for the DC in this case is 6 %, which shows 12 % reduction in the overshoot value compared to the results with conventional PI controller. The settling time also decreased from 300 ms to 200 ms. For a detailed comparison, DC voltage dynamic response for both non-linear PI and conventional PI is depicted in Fig 8(b).

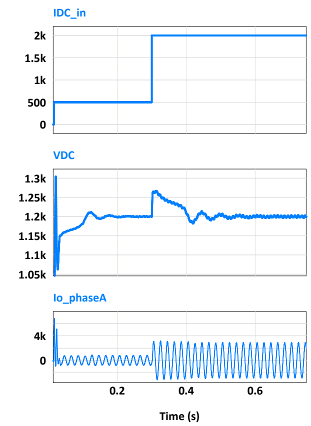

(a) Input current, DC voltage, and output current

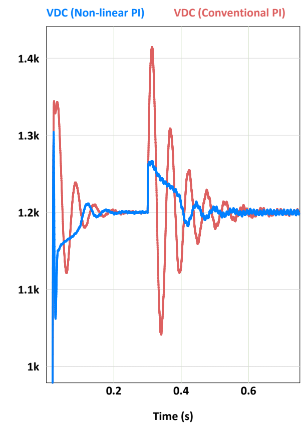

(b) DC voltage for non-linear PI vs conventional PI

Fig. 8. Simulation results with non-linear PI controller in large step changes.

By comparing phase A output current waveforms in Figs. 4(b) and 8(a), a notable improvement in the inner loop can be observed. Since the reference current is produced by the voltage loop controller, output control of the non-linear PI controller leads to an improved dynamic response in the inner loop and current reference as well. Maximum current overshoot is decreased from 50 % to 10 %, and it stabilizes in less cycles, compared to conventional PI controller.

IV. Hardware Validation

A CHIL test is performed to test the functionality of the digital non-linear PI controller in a more realistic case. A Typhoon HIL real-time simulator is used to emulate the power stage with 1 μs time step. A TMS320F28379D DSP is utilized to implement the non-linear PI controller code. Two ePWM modules and 7 ADC channels are programmed to setup the control system. ePWM1 is for triggering the ADC conversion, and ePWM2 is generating three-phase SPWM pulses. An interrupt is enabled in the Peripheral Interrupt Expansion (PIE) to call Interrupt Service Routine (ISR) function at the end of conversion of ADC channels.

The predefined non-linear functions are initialized in the DSP, and called at each ISR function. The ePWM1 clock is set to 250 μs, and the PI transfer function is discretized using Tustin's method and same sampling time (250 μs).

The results for conventional PI and non-linear PI are provided in Fig. 9, in which Figs 9(a) and (b) show the DC input current step change and DC voltage dynamic response. A comparison for DC voltage with conventional and non-linear PI controller is provided in Fig. 9(c) that verifies its enhanced dynamic response. The overshoot and settling time are decreased by 12 % and 33 %, respectively. The CHIL result matches with the simulation results, and verifies the operation of embedded non-linear controller in DSP.

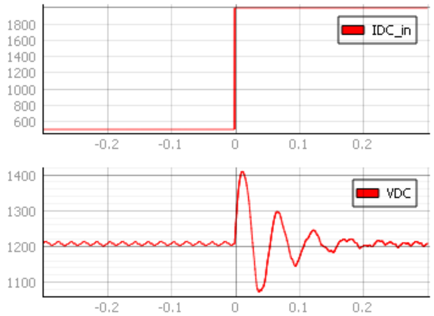

(a) Conventional PI controller

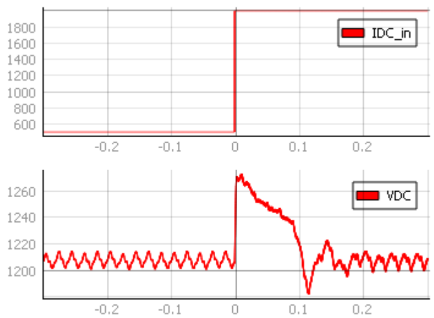

(b) Non-linear PI controller

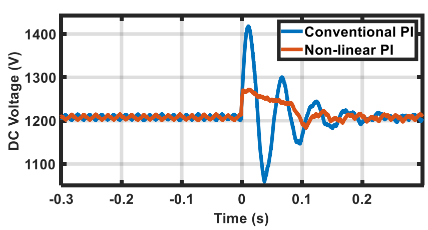

(c) DC voltage dynamic response comparison

Fig. 9. CHIL results: DC voltage at large step changes.

V. Conclusion

This paper proposes a non-linear PI controller for improving dynamic response of DC-AC converters in the application of SMG with HESS, where fast and precise dynamic response for very large step changes is critical. The non-linear PI controller adjusts the PI gains at each step based on the error value and predefined non-linear functions. This adaptive control system shows significant improvement in dynamic response of DC voltage and output current, especially in large variations of the SMG operation in manoeuvring phase. Compared to a benchmark case with conventional PI controller, overshoots and settling time decreased by 12 % and 33 %, respectively. A frequency-domain analysis is done to design non-linear functions, and ensure stable operation in all states. Simulations and CHIL tests are performed to evaluate and verify the controller performance.

References

[1] L. Xu et al., "A Review of DC Shipboard Microgrids—Part I: Power Architectures, Energy Storage, and Power Converters," in IEEE Transactions on Power Electronics, vol. 37, no. 5, pp. 5155-5172, May 2022, doi: 10.1109/TPEL.2021.3128417.

[2] L. Xu et al., "A Review of DC Shipboard Microgrids—Part II: Control Architectures, Stability Analysis, and Protection Schemes," in IEEE Transactions on Power Electronics, vol. 37, no. 4, pp. 4105-4120, April 2022, doi: 10.1109/TPEL.2021.3128409.

[3] P. Ghimire, D. Park, M. K. Zadeh, J. Thorstensen and E. Pedersen, "Shipboard Electric Power Conversion: System Architecture, Applications, Control, and Challenges [Technology Leaders]," in IEEE Electrification Magazine, vol. 7, no. 4, pp. 6-20, Dec. 2019, doi: 10.1109/MELE.2019.2943948.

[4] M. A. Hassan et al., "DC Shipboard Microgrids With Constant Power Loads: A Review of Advanced Nonlinear Control Strategies and Stabilization Techniques," in IEEE Transactions on Smart Grid, vol. 13, no. 5, pp. 3422-3438, Sept. 2022, doi: 10.1109/TSG.2022.3168267.

[5] L. Yacoubi, K. Al-Haddad, L. -A. Dessaint and F. Fnaiech, "Linear and Nonlinear Control Techniques for a Three-Phase Three-Level NPC Boost Rectifier," in IEEE Transactions on Industrial Electronics, vol. 53, no. 6, pp. 1908-1918, Dec. 2006, doi: 10.1109/TIE.2006.881990.

[6] Krein P. T. (2015). Elements of power electronics (Second). Oxford University Press.

[7] J. Rodriguez and P. Cortes, Predictive Control of Power Converters and Electrical Drives. Wiley-IEEE Press, 2012.

[8] R. E. Pérez-Guzmán, M. Rivera and P. W. Wheeler, "Recent Advances of Predictive Control in Power Converters," 2020 IEEE International Conference on Industrial Technology (ICIT), 2020, pp. 1100-1105, doi: 10.1109/ICIT45562.2020.9067169.

[9] J. Han, "From PID to Active Disturbance Rejection Control," in IEEE Transactions on Industrial Electronics, vol. 56, no. 3, pp. 900-906, March 2009, doi: 10.1109/TIE.2008.2011621.

[10] V. Yousefzadeh and S. Choudhury, "Nonlinear digital PID controller for DC-DC converters," 2008 Twenty-Third Annual IEEE Applied Power Electronics Conference and Exposition, Austin, TX, USA, 2008, pp. 1704-1709, doi: 10.1109/APEC.2008.4522956.

[11] Q. Zhang and Y. Huo, "A Self-Tuning Method of PI Controllers for DC/AC Inverters Based on Energy Balance Algorithm," 2024 IEEE 10th International Power Electronics and Motion Control Conference (IPEMC2024-ECCE Asia), Chengdu, China, 2024, pp. 5099-5104, doi: 10.1109/IPEMC-ECCEAsia60879.2024.10567296.

[12] A. Bouhouta, S. Moulahoum, N. Kabache and I. Colak, "Adaptive PI Control Strategy Based on Fuzzy Logic for an Active Harmonic Compensator," 2020 9th International Conference on Renewable Energy Research and Application (ICRERA), Glasgow, UK, 2020, pp. 326-331, doi: 10.1109/ICRERA49962.2020.9242734.

[13] A. R. Nair, R. Bhattarai, M. Smith and S. Kamalasadan, "A Hybrid Adaptive Control Architecture for Grid-Connected Inverter With Optimal Policy Generation," in IEEE Transactions on Industry Applications, vol. 58, no. 1, pp. 855-867, Jan.-Feb. 2022, doi: 10.1109/TIA.2021.3123559.

[14] Texas Instruments, "spruid3," https://www.ti.com/lit/pdf/spruid3

[15] M. Bhardwaj and C. Jiang, "Vienna Rectifier-Based, Three-Phase Power Factor Correction (PFC) Reference Design Using C2000™ MCU", Texas Instruments, "TIDM-1000 Reference Design," https://www.ti.com/tool/TIDM-1000

[16] R. Shi, S. Semsar and P. W. Lehn, "Single-Stage Hybrid Energy Storage Integration in Electric Vehicles Using Vector Controlled Power Sharing," in IEEE Transactions on Industrial Electronics, vol. 68, no. 11, pp. 10623-10633, Nov. 2021, doi: 10.1109/TIE.2020.3038100.

[17] R. Peña-Alzola, M. Liserre, F. Blaabjerg, M. Ordonez and Y. Yang, "LCL-Filter Design for Robust Active Damping in Grid-Connected Converters," in IEEE Transactions on Industrial Informatics, vol. 10, no. 4, pp. 2192-2203, Nov. 2014, doi: 10.1109/TII.2014.2361604.

[18] Liserre *, M., Blaabjerg, F., & Dell'Aquila, A. (2004). Step-by-step design procedure for a grid-connected three-phase PWM voltage source converter. International Journal of Electronics, 91(8), 445–460. https://doi.org/10.1080/00207210412331306186

[19] V. Blasko and V. Kaura, "A new mathematical model and control of a three-phase AC-DC voltage source converter," in IEEE Transactions on Power Electronics, vol. 12, no. 1, pp. 116-123, Jan. 1997, doi: 10.1109/63.554176.